

## Electronic Supplementary Information (ESI)

for

### A Two-Point Fluorescence Detection Flow Cell with Empirical Calibration for High Optical Density Analysis

Tin Weitner<sup>1,2</sup> and Davor Šakić<sup>1,2</sup>

---

1. University of Zagreb Faculty of Pharmacy and Biochemistry, Ante Kovačića 1, 10000 Zagreb, Croatia  
2. TINFE HTS llc., Haviđićeva 24, 10010 Zagreb, Croatia

This ESI provides additional methodological and computational details, including flow-cell fabrication, effective path length stability, raw-data processing, and a fully reproducible Excel Solver implementation of the calibration/optimization procedure.

Raw and processed datasets are available in this Zenodo repository (DOI: 10.5281/zenodo.18393535).

#### Contents

- S1. Flow-cell fabrication
- S2. Effective optical path length
- S3. Notes on fluorophore choice
- S4. Calibration model and Excel Solver implementation
- S5. Static-sample dataset: structure and reported performance metrics
- S6. Continuous-flow gradient dataset: UV-based gradient reconstruction and delay correction

## S1. Flow-cell fabrication

The first flow-cell prototype was fabricated by stereolithography (SLA) 3D printing on a Formlabs Form 3 printer using Formlabs Durable Resin. The transparent resin was intentionally chosen to enable visual inspection of internal channel alignment, sealing, and optical-port placement during early prototyping. During measurements, stray light was suppressed by fully wrapping the assembled cell body with an opaque black plastic sheet, eliminating ambient and lateral light leakage. Quartz ball lenses mounted in the optical ports define the excitation/emission beam paths and the printed polymer apparently does not serve as an optical waveguide.

## S2. Effective optical path length

In the presented geometry, the effective optical path lengths to the two fluorescence detection points are governed by the fixed CAD-defined distances between optical ports and the internal channel diameter. Because beam shaping and collection are set by the quartz ball lenses and fiber alignment, the polymer body does not define (or guide) the optical path. Across independently printed parts, dimensional deviations were within typical SLA tolerances (sub-100  $\mu\text{m}$  scale), corresponding to <1% variation in the geometric source-to-detector distances.

## S3. Notes on fluorophore choice

Quinine sulfate is a useful complementary fluorophore because it exhibits a large Stokes shift (typically  $\sim 100$  nm, depending on solvent and pH), which reduces emission re-absorption and therefore down-weights secondary inner-filter contributions. Fluorescein has a medium Stokes shift (typically  $\sim 20$ – $30$  nm), with greater absorption–emission overlap and stronger susceptibility to secondary IFE.

## S4. Calibration model and Excel Solver implementation

The calibration uses a parametric model linking concentration ( $c$ ) to two fluorescence signals measured at fixed positions ( $F_0$  and  $F_1$ ). For the two-point case, the model is implemented as:

$$F_{\text{IFE\_CORR}} = F_0^{1+q_1} \cdot F_1^{-q_1}$$

for which  $q_1$  parameter is optimized to get the best linear fit for equation

$$F_{\text{IFE\_CORR}} = p_0 + p_1 \cdot c$$

where  $q_1$  is an empirically optimized exponent and  $p_0, p_1$  are linear calibration parameters obtained from least-squares fitting of  $F_{\text{IFE\_CORR}}$  versus concentration.

Excel Solver implementation:

1) Compute the corrected signal:

$$F_{\text{IFE\_CORR}} = F_0^{1+q_1} \cdot F_1^{-q_1}; \text{ set } q_1 \text{ to 1 in separate cell.}$$

2) Normalize corrected signal:  $F_{\text{IFE\_CORR\_norm}} = F_{\text{IFE\_CORR}} / \max(F_{\text{IFE\_CORR}})$ .

3) Define excel functions RSQ ( $r^2$ ), SLOPE ( $p_1$ ), INTERCEPT ( $p_0$ ), and STEYX on the data.

4) Define the objectives: coefficient of determination ( $r^2$ ) and/or RSS as the sum of squared residuals between  $c_{\text{norm}}$  and  $F_{\text{IFE\_CORR\_norm}}$ :

$$\text{RSS} = \sum (c_{\text{norm}} - (F_{\text{IFE\_CORR\_norm}} - p_0)/p_1)^2$$

5) Optimization can be performed using standard nonlinear optimization routines (e.g., spreadsheet Solver tools) to minimize residual error or maximize goodness-of-fit.

6) Report  $R^2$ , slope/intercept, and LOD metrics using standard linear-regression outputs.

7) Normalize concentration and signals (optional):

$$c_{\text{norm}} = c / \max(c); F_{0\_norm} = F_0 / \max(F_0, F_1); F_{1\_norm} = F_1 / \max(F_0, F_1)$$

## S5. Static-sample dataset

The static dataset workbook contains the following sheets: (i) OceanOptics-import (raw spectra import), (ii) Dark-corrected, (iii) SG-filtered, and (iv) F\_IFE-CORR (signal extraction at the selected emission wavelength and calibration).

The F\_IFE-CORR sheet includes the normalized concentration axis, extracted fluorescence intensities (F0 and F1), the computed corrected signal, and the Solver objective (RSS). Performance metrics ( $R^2$ , LOD, LOD%, and slope error) are calculated from linear regression of the corrected signal versus concentration across the full dilution series.

## S6. Continuous-flow gradient dataset

Continuous-flow gradients were generated on an ÄKTA start system using a programmed 0–100% B gradient at  $1.0 \text{ mL min}^{-1}$  and monitored by the built-in UV detector at 280 nm (0.2 cm optical path). To obtain a corrected concentration axis, the recorded UV280 trace was baseline-corrected (baseline defined as the mean of the first 20 points prior to gradient initiation) and then mapped to effective %B composition. The method export indicates a gradient delay volume of 0.10 mL; this delay can be applied as a time/volume shift to align the UV-derived composition at the flow cell with the programmed gradient. In addition,

mixer dispersion (static mixer volume 0.40 mL) leads to mild nonlinearity at the gradient start/end; therefore, only the central 2–98% region was used for IFE analysis in the main manuscript.

Summary from the supplied ÄKTA chromatogram export:

UV<sub>280</sub> trace max = 146.25 mAU; baseline (first 20 pts) = 0.14 mAU; flow rate = 1.00 mL min<sup>-1</sup>; gradient delay volume = 0.10 mL; mixer volume = 0.40 mL.

## S7. Additional datasets

The following datasets provide supplementary validation of the two-point fluorescence calibration under conditions that extend beyond the primary flow experiment described in the main manuscript. Specifically, the influence of flow rate and fluorophore-dependent photophysical properties on calibration performance were evaluated.

For fluorescein, an additional continuous-flow gradient experiment was performed at a reduced flow rate (0.5 mL·min<sup>-1</sup>) to assess the effect of hydrodynamic conditions (residence time, axial dispersion, and gradient steepness) on the calibration parameters and resulting linearity. This dataset enables direct comparison with the 1.0 mL·min<sup>-1</sup> experiment presented in the main text, isolating the role of flow-dependent transport phenomena in shaping the raw fluorescence signals ( $F_0$ ,  $F_1$ ) and the optimized correction exponent ( $q_1$ ).

To examine the generality of the calibration approach across fluorophores with different optical properties, a complementary dataset was acquired using quinine sulfate (QS) at 0.5 mL·min<sup>-1</sup>. In contrast to fluorescein, quinine sulfate exhibits a substantially larger Stokes shift and reduced spectral overlap between absorption and emission, thereby diminishing secondary inner-filter effects. This system provides a useful test case for evaluating the method under conditions where signal attenuation is weaker, but fluorescence intensity and signal-to-noise ratio are lower.

Together, these datasets probe two key aspects of the method: (i) robustness of the calibration under varying flow conditions, and (ii) sensitivity of the correction model to fluorophore-specific emission characteristics and noise levels.

The raw fluorescence signals ( $F_0$  and  $F_1$ , denoted  $F_x$ ) are expressed in spectrophotometer detector counts (CCD counts), corresponding to integrated emission intensity over the selected wavelength window. The corrected fluorescence signal ( $F_{\text{IFE\_CORR}}$ ) retains the same dimensionality as the raw signals and can also be expressed in detector counts. However, despite this formal unit consistency,  $F_{\text{IFE\_CORR}}$  should still be interpreted as a derived, model-dependent signal, and quantitative meaning arises only after calibration against concentration.

### S7.1. Fluorescein (flow 0.5 mL/min)

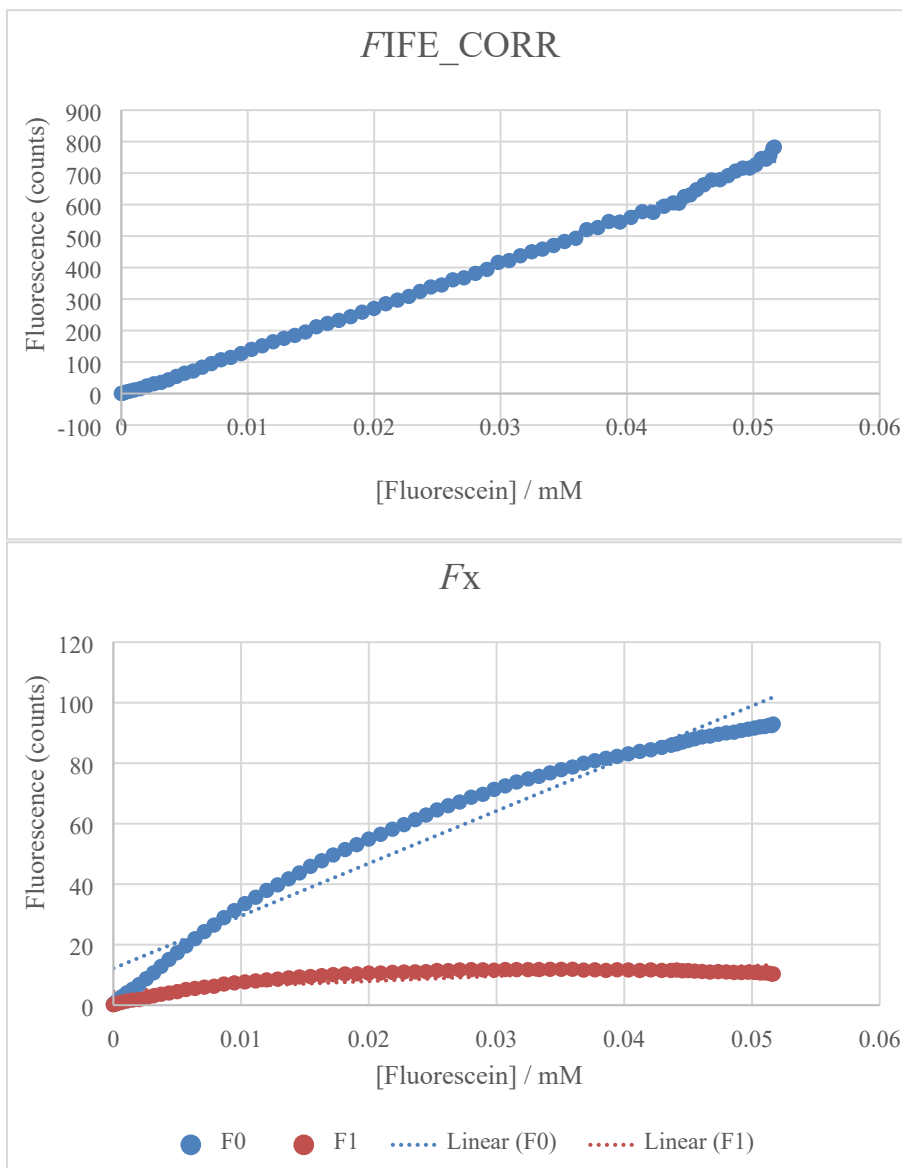


**Figure S1.** Fluorescence signals and calibrated response for fluorescein under continuous-flow gradient conditions at  $0.5 \text{ mL}\cdot\text{min}^{-1}$ . **Top:** Corrected fluorescence signal ( $F_{\text{IFE\_CORR}}$ ) as a function of normalized concentration, showing strong linearity ( $R^2 = 0.9975$ ). **Bottom:** Raw fluorescence signals ( $F_x$ ) at the two detection points ( $F_0$  and  $F_1$ ) with corresponding linear fits, illustrating pronounced nonlinearity due to inner-filter effects ( $R^2(F_0) > 0.9531$ ,  $R^2(F_1) = 0.6466$ ). The calibrated signal restores a linear fluorescence–concentration relationship across the full gradient range, demonstrating effective compensation of position-dependent attenuation at reduced flow rate.

## S7.2. Quinine sulfate (flow 0.5 mL/min)

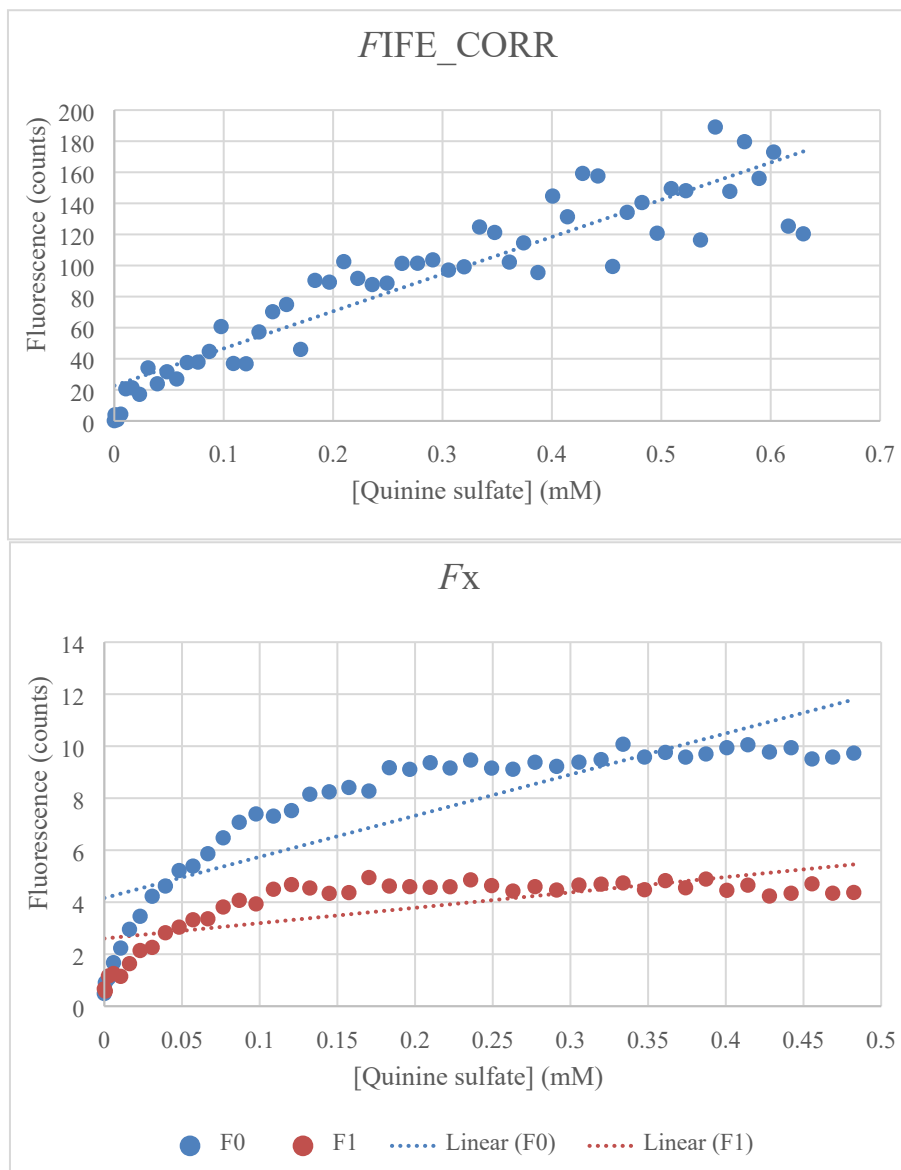


**Figure S2.** Fluorescence signals and calibrated response for quinine sulfate under continuous-flow gradient conditions at 0.5 mL·min<sup>-1</sup>. **Top:** Corrected fluorescence signal ( $F_{\text{IFE\_CORR}}$ ) as a function of normalized concentration, yielding partial linearization ( $R^2 = 0.8652$ ). **Bottom:** Raw fluorescence signals ( $F_x$ ) at the two detection points ( $F_0$  and  $F_1$ ) with corresponding linear fits, illustrating pronounced nonlinearity due to inner-filter effects ( $R^2(F_0) > 0.07070$ ,  $R^2(F_1) = 0.5065$ ). The reduced performance relative to fluorescein reflects lower fluorescence intensity and increased noise propagation in the correction model.

### S7.3. Calibration parameters and analytical performance metrics for all datasets

**Table S1.** Summary of fitted calibration parameters and analytical performance metrics obtained for static and flow experiments with fluorescein (FL) and quinine sulfate (QS). Parameters  $q_1$ ,  $p_0$ , and  $p_1$  correspond to the optimized empirical model coefficients. The coefficient of determination ( $R^2$ ) quantifies linearity of the corrected fluorescence signal. Limits of detection (LOD) are reported in concentration units (mM) and as a percentage of the investigated concentration range (LOD%). The relative slope error (mErr%) reflects deviation from ideal proportionality after calibration.

<b>Dataset</b>	<b><math>q_1</math></b>	<b><math>p_0</math></b>	<b><math>p_1</math></b>	<b><math>R^2</math></b>	<b>LOD / mM</b>	<b>LOD% (%)</b>	<b>mErr% (%)</b>
Fluorescein (static)	3.021	-10.1	15354	0.99812	0.0021	5.7	0.5
Fluorescein (flow, 0.5 mL·min <sup>-1</sup> )	0.970	-12.3	14509	0.99750	0.0029	5.6	-4.2
Fluorescein (flow, 1.0 mL·min <sup>-1</sup> )	1.310	15.6	66467	0.99669	0.0030	6.3	2.1
Quinine sulfate (flow, 0.5 mL·min <sup>-1</sup> )	3.338	22.7	239.3	0.86524	0.2635	41.8	-6.9